Available online at www.sciencedirect.com

ScienceDirect

Acta Materialia 61 (2013) 7098–7108

Acta MATERIALIA

www.elsevier.com/locate/actamat

Influence of Cr on the nucleation of primary Al and formation of twinned dendrites in Al–Zn–Cr alloys: Can icosahedral solid clusters play a role?

Güven Kurtuldu [a,*], Philippe Jarry [b], Michel Rappaz [a]

[a] Computational Materials Laboratory, Institute of Materials, Ecole Polytechnique Fédérale de Lausanne, Station 12, CH-1015 Lausanne, Switzerland
[b] Constellium CRV, ZI Centr'alp, 0725 rue Aristide Bergès, BP 27, Voreppe FR-38341, France

Received 22 May 2013; accepted 26 July 2013
Available online 3 September 2013

Abstract

The equiaxed solidification of Al–20 wt.% Zn alloys revealed an unexpectedly large number of fine grains which are in a twin, or near-twin, relationship with their nearest neighbors when minute amounts of Cr (1000 ppm) are added to the melt. Several occurrences of neighboring grains sharing a nearly common ⟨1 1 0⟩ direction with a fivefold symmetry multi-twinning relationship have been found. These findings are a very strong indication that the primary face-centered cubic Al phase forms on either icosahedron quasicrystals or nuclei of the parent stable $Al_{45}Cr_7$ phase, which exhibits several fivefold symmetry building blocks in its large monoclinic unit cell. They are further supported by thermodynamic calculations and by grains sometimes exhibiting orientations compatible with the so-called interlocked icosahedron. These results are important, not only because they provide an explanation of the nucleation of twinned dendrites in Al alloys, a topic that has remained unclear over the past 60 years despite several recent investigations, but also because they identify a so far neglected nucleation mechanism in aluminum alloys, which could also apply to other metallic systems.

Keywords: Quasicrystal; Nucleation; Twinned dendrites; Solidification; Aluminum alloys

1. Introduction

Twinned dendrites, also called feathery grains, have been known for more than 60 years in direct chill (DC) cast Al alloys. They are considered as defects (or undesirable microstructures), due to their strongly anisotropic properties [1,2]. Using electron backscatter diffraction (EBSD), Henry et al. [3–6] clearly identified the crystallographic relationships of such growth morphologies: a feathery grain is made of a series of alternated twinned and untwinned lamellae, separated by coherent–straight and incoherent–wavy twin boundaries (see Fig. 1). The coherent {1 1 1} twin boundaries are located at the center of twinned dendrite trunks growing along ⟨1 1 0⟩ directions, while secondary dendrite arms on the twinned/untwinned side of each trunk also grow generally along ⟨1 1 0⟩ directions and impinge with the untwinned/twinned side arms of the two neighbor dendrites, thus creating the incoherent wavy twin boundaries.

Up to now, the formation of twinned dendrites was shown to occur under specific solidification conditions which can be summarized as follows [6–9]: (i) poor or no inoculation of the alloy (in order to prevent the formation of equiaxed grains); (ii) high thermal gradient (typically 100 K cm^{-1}) and cooling rate (typically 10 K s^{-1}) (i.e., growth rate of typically 1 mm s^{-1}); (iii) strong convection of hot liquid (e.g. associated with pouring) insofar as it promotes high gradient at the front, as convection induced by stirring drastically decreases the thermal gradient in the liquid and does not promote the formation of twinned dendrites. It is known in industry that some aluminum alloys

* Corresponding author. Tel.: +41 216933943.
E-mail address: guven.kurtuldu@epfl.ch (G. Kurtuldu).

1359-6454/$36.00
http://dx.doi.org/10.1016/j.actamat.2013.07.056

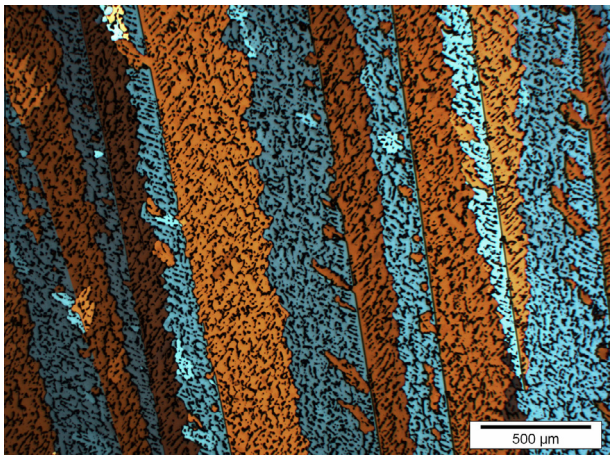

Fig. 1. Twinned dendrites formed in a directionally solidified Al–12 wt.% Zn alloy.

are more prone to feathery grains formation than others, but the role of the nature and amount of alloying elements is still not understood. For example, Salgado-Ordorica and Rappaz [7] could produce twinned dendrites in different binary Al alloys with solute elements having a low/high stacking fault energy (Cu and Ni, respectively) or solidifying with a hexagonal close packed structure (Mg and Zn), providing the other conditions were met. Surprisingly, these authors could not produce twinned dendrites in Al–Zn for compositions higher than 40 wt.%, for which "regular" dendrites (i.e., untwinned) are known to grow not along ⟨100⟩ directions, as do most cubic-symmetry metals, but along directions which are closer to ⟨110⟩ [10,11]. Concerning convection, DC cast billets with lateral liquid feeding exhibited twinned dendrites in regions where the shearing rate was highest [6]. In directional solidification (DS), twinned dendrites did not form by stirring the melt, but they did form if the melt was poured on the chill plate [12]. However, the role of convection is still unclear. More confusion has been brought recently by Li et al. [13], who observed that the application of a static magnetic field of only 0.2 T, which is supposed to weaken convection, induces the formation of twinned dendrites in Al–Fe and Al–Zn alloys in small DC cast ingots. Finally, although twinned dendrites have a growth advantage over regular dendrites under the above-mentioned conditions, there is still some uncertainty about their tip morphology [3,12,14–18]. More important, nothing is known about twin nucleation. It was conjectured that they are initiated by stacking faults forming during growth, but no experimental evidence was ever provided.

The present study was actually initiated with the aim of investigating the effect of minute additions of chromium on dendritic growth in Al–20 wt.% Zn alloy. This specific composition was selected because it has been shown to be the upper limit for which ⟨100⟩ dendrites are observed. Above this composition, the system exhibits a dendrite orientation transition (DOT), i.e., a gradual transition from ⟨100⟩ to ⟨110⟩, which has been interpreted as a modification of the solid–liquid interfacial energy anisotropy [10,11,19]. In DS Al–20 wt.% Zn, we already found that minute additions of Cr (typically 200 to 1000 ppm) drastically modify the dendrite growth direction from ⟨100⟩ to ⟨110⟩, but the reason in this case is less clear [20]. In order to further examine the effect of chromium additions in Al–Zn, equiaxed solidification (ES) was achieved under nearly uniform temperature. The results of this work are presented in the present paper. We show that a surprisingly large number of twinned grains are formed in ES Al–20 wt.% Zn–0.1 wt.% Cr alloy (nearly nil convection and thermal gradient), i.e., under conditions which contradict all previously reported experimental findings. By detailed crystal orientation correlations, we show that twinning in this case is most likely initiated by an icosahedral quasicrystal (iQC) phase, or its approximant stable phase $Al_{45}Cr_7$. QCs exhibit a fivefold symmetry while the stable phase has a large monoclinic cell with many fivefold symmetry building blocks in its unit cell. There is fairly strong evidence that such phases could act as a template for the formation of the primary phase, with many twin relationships. This mechanism sheds some new light on the formation of twinned dendrites in DC cast Al alloys, since iron is very often present in technical Al alloys and Al–Fe can also form QCs [21]. Its contribution to the inoculation of liquid aluminum alloys (or other face-centered cubic (fcc) metals) should also be considered.

2. Materials and experimental procedure

Al–Zn–Cr alloys were prepared from the pure elements (99.99 wt.% purity) in a vacuum induction furnace and under Ar atmosphere in order to ensure complete mixing of the components. Specimens, typically 200 mm long and 3.9 mm in diameter, were extracted from the ingot and inserted into a quartz tube. Remelting and solidification of the specimens were then performed in a vertical furnace, with both ends covered by thick insulating wool caps, thus ensuring nearly isothermal growth conditions. The temperature of the furnace was initially adjusted 50 K above the liquidus temperature of the alloy. After complete melting, the furnace was turned off and left to cool down slowly. The temperature evolution, recorded by a thermocouple, exhibits a recalescence, typical of solidification of a melt of nearly uniform temperature. The cooling rate of the melt before recalescence was $\sim -0.2\ K\ s^{-1}$. At some point of solidification after recalescence, the specimen was quenched in a water tank to observe the microstructure at room temperature.

Longitudinal sections of the specimens were observed using optical microscopy, scanning electron microscopy (SEM) and EBSD analysis in order to correlate the solidification morphology and the crystallographic orientation. For that purpose, the samples were cut transversally into 4 cm long cylinders and then longitudinal surfaces were mirror-polished and etched with a dilute Keller solution for a few seconds to reveal the microstructure. For EBSD analysis, after the surface was polished with 0.25 μm

diamond particle paste, it was electropolished with a standard A2-Struers solution (4 V for 10 s and 25 V for 2 s) to remove the top surface layer deformed during mechanical polishing. EBSD measurements were performed using Phillips XLF-30 FEG SEM enhanced with an HKL detector. On EBSD maps, grain boundaries were identified using a minimum disorientation angle of 5° between adjacent pixels. Chemical composition analyses were performed using SEM coupled with energy-dispersive X-ray spectroscopy.

3. Results

3.1. A large twin dendrite in an Al–Zn–Cr specimen solidified under equiaxed conditions

In order to verify that the effect seen on the microstructure was indeed due to the 0.1wt.% Cr, experiments with and without chromium additions were made. As a reference case, Fig. 2 shows the microstructure of an Al–20 wt.% Zn alloy solidified under nearly isothermal conditions. As can be seen, the primary and secondary dendrite arms have grown at 90° in this section, which incidentally nearly coincides with a {001} plane of the specimen. It was verified that these arms correspond to ⟨100⟩ directions, i.e., to the expected growth directions of fcc metals and of aluminum–zinc alloys below 25 wt.% concentration [10].

Adding now 0.1 wt.% Cr to an Al–20 wt.% Zn specimen solidified under identical thermal conditions produces the microstructure shown in Fig. 3a. In this longitudinal section, the specimen is made of two different microstructures: most of the section exhibits well-oriented long dendrites, while both ends show small equiaxed-globular dendrites, with ill-defined growth directions.[1] These two microstructures are enlarged in Fig. 3b and c. We first focus on the longer grain for which the dendrite growth directions can be identified and compared with those of Fig. 2.

From the impingement of some of the dendrite arms in Fig. 3b, it can be inferred that the large grain seems to have grown from left to right until it was stopped by the small equiaxed grains on the right of Fig. 3a. The growth within this grain has proceeded with an alternation of two main dendrite growth directions making an angle of 60° in this plane. A few arms visible on the left of Fig. 3b have grown in the direction perpendicular to the axis of the cylindrical specimen in this section and also make an angle of 60° with the former two, more frequent, directions. The average secondary arm spacing of these dendrites is ~85 μm, in good agreement with calculated value for the given cooling rate. Therefore, at first sight, this long grain is made of ⟨110⟩ dendrite arms seen in a {111} plane, the axis of the cylindrical specimen being close to a ⟨112⟩ direction of this grain. This observation, which already is surprising (compare Figs. 2 and 3b), would confirm the effect of small Cr additions seen in Bridgman experiments [20], i.e., a switch of the dendrite growth direction from ⟨100⟩ to ⟨110⟩. However, as shown hereafter, these ⟨110⟩ dendrites are twinned in the present case, which is even more surprising.

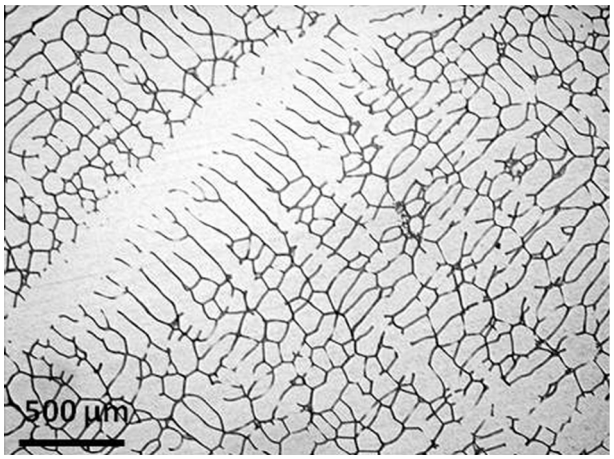

Fig. 2. Microstructure of an Al–20 wt.% Zn alloy solidified under ES conditions, clearly showing ⟨100⟩ primary and secondary arms having grown at 90°.

The crystallographic orientation of this long dendrite was measured by EBSD in the rectangular domain of the section shown in Fig. 3a. The reconstructed orientation map of this region is superimposed on the actual micrograph in Fig. 3d. The violet and green colors correspond to the three Euler angles. The corresponding ⟨110⟩ pole figure in Fig. 3e confirms the observations made on the metallographic sections of Fig. 3b: three ⟨110⟩ directions are located on the circle of the stereographic projection (highlighted by small circles) and correspond to the dendrite growth directions seen in Fig. 3b. Thus, the section corresponds indeed to a {111} plane as shown in Fig. 3f, where one ⟨111⟩ direction surrounded by a small circle is almost at the center of the stereographic projection. However, the other three ⟨110⟩ directions located near the center of the stereographic projection are in fact doubled and are in a twin relationship. The three green points corresponding to the green region in Fig. 3d are in a symmetric relationship with the violet ⟨110⟩ directions corresponding to the violet zone of Fig. 3d, when we consider the {111} twin plane.

This twin relationship can also be seen in the ⟨111⟩ pole figure, where the three non-common ⟨111⟩ directions have symmetric relationship with respect to the {111} twin plane. The fact that both orientations of the twinned and untwinned parts can be seen in the same section is due to the fact that the section is not exactly parallel to the {111} plane. Indeed, in the top and bottom parts of the EBSD map, one has predominantly one of the two colors.

In order to fully elucidate this twinned morphology, a section perpendicular to that of Fig. 3 was made. Fig. 4a

[1] Similar equiaxed grains were observed in specimens solidified without chromium, but with a larger grain size. Although their formation mechanisms were not explored further, they could result from some dendrite fragmentation/detachment and then floatation or sedimentation (the density of the solid close to the liquidus temperature is actually very close to that of the liquid for an Al–20 wt.% Zn, due to the partitioning of the heavy zinc solute elements).

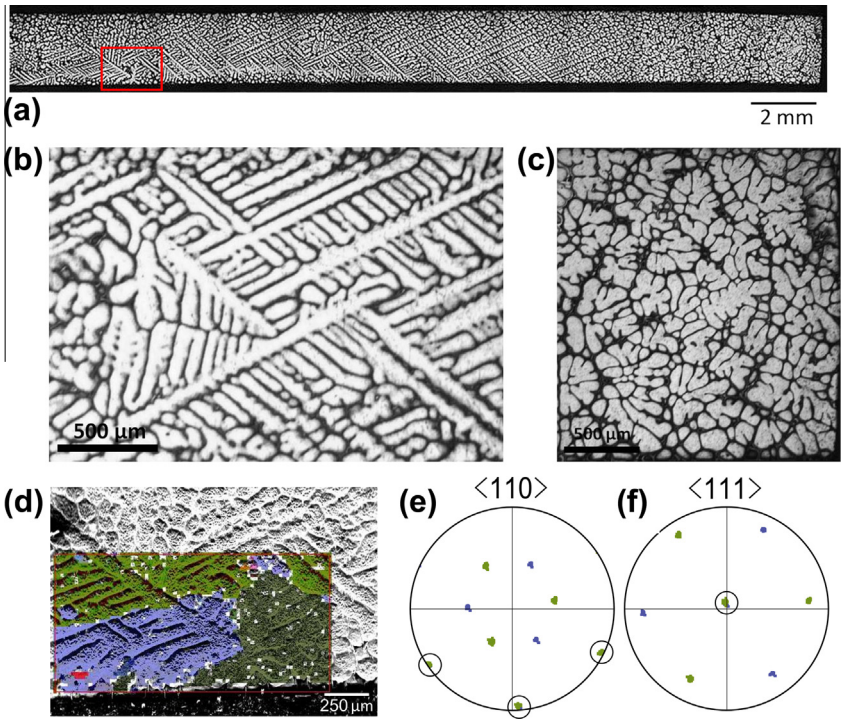

Fig. 3. (a) Microstructure of Al–20 wt.% Zn–0.1 wt.% Cr alloy solidified under the same conditions as the specimen shown in Fig. 2. (b) Enlarged view of the large dendritic grain seen in (a), showing primary and secondary arms having grown at 60°. (c) Enlarged view of the equiaxed region shown in (a). (d) Secondary electron SEM image of the section indicated by the red rectangle in (a) and EBSD map with the corresponding (e) ⟨1 1 0⟩ and (f) ⟨1 1 1⟩ pole figures. In these pole figures, the normal to the specimen surface is at the center, and one ⟨1 1 1⟩ direction is very close to the center (small circle in the ⟨1 1 1⟩ pole figure). The ⟨1 1 0⟩ growth directions of the dendrite arms are also circled in the ⟨1 1 0⟩ pole figure.

shows the microstructure in a section perpendicular to the common {1 1 1} plane. The straight coherent twin plane separating the twinned and untwinned parts of the dendrite can be discerned by the gray contrast of this SEM image. In Fig. 4b, a false-color EBSD map shows these two parts in blue and pink, while a few equiaxed grains near the twinned dendrite appear in brown and bright blue. The ⟨1 1 0⟩ and ⟨1 1 1⟩ pole figures of Fig. 4c and d, corresponding to the twinned dendrite only, demonstrate the twin relationship with a common {1 1 1} twin plane and three common ⟨1 1 0⟩ dendrite growth directions (again circled in this figure).

It is known that twinned dendrites have a growth advantage over regular dendrites, i.e. the undercooling of the twinned dendrite tip is smaller than that of regular columnar dendrites [22]. Formation of such a long twinned dendrite (Fig. 3a) in our alloy indicates a growth advantage over the nucleation of equiaxed grains. Another example of a long twinned dendrite embedded in an otherwise equiaxed grain structure is provided in Fig. 2 of Ref. [23] for a grain-refined Al–Mg alloy.

3.2. Fine equiaxed grain structure exhibiting many twin relationships

Fig. 5a shows a longitudinal section of the microstructure of another Al–20 wt.% Zn–0.1 wt.% Cr alloy solidified under the same ES conditions. In Fig. 5b, the EBSD relative Euler orientation map clearly reveals that this microstructure is made of fine equiaxed grains of ~100 μm in diameter, even though, like the other specimen, it was not inoculated with TiB_2. Four pairs of grains, labeled 1 to 4, are identified in this reconstructed map. Their ⟨1 1 0⟩ and ⟨1 1 1⟩ pole figures are shown in Fig. 5c–f. As can be seen in Fig. 5c and d, there is an exact twin relationship between grains 1A and 1B and between grains 2A and 2B. In both situations, the two pairs of grains share one common ⟨1 1 1⟩ direction and three common ⟨1 1 0⟩ directions (circled in these pole figures). The other non-common ⟨1 1 0⟩ and ⟨1 1 1⟩ directions are in a symmetric relationship with respect to the common {1 1 1} twin plane (defined by an arc of a circle). The pole figures of Fig. 5e and f, corresponding to the pairs of grains 3A and 3B and 4A and 4B, present a crystallographic relationship close to a twin relationship that will be called hereafter "near-twin". As can be seen, one ⟨1 1 1⟩ direction and two ⟨1 1 0⟩ directions of these pairs of grains are nearly coinciding (simple circles), but the nearly common {1 1 1} planes are slightly rotated around a third common ⟨1 1 0⟩ direction (double circle in these pole figures). Taking into account this small rotation, the other directions are in a nearly symmetric relationship with respect to the nearly common {1 1 1} plane. In other words, the near-twin relationship can be decomposed into: (i) a twin symmetric relationship with respect to a common {1 1 1} plane; (ii) a small rotation

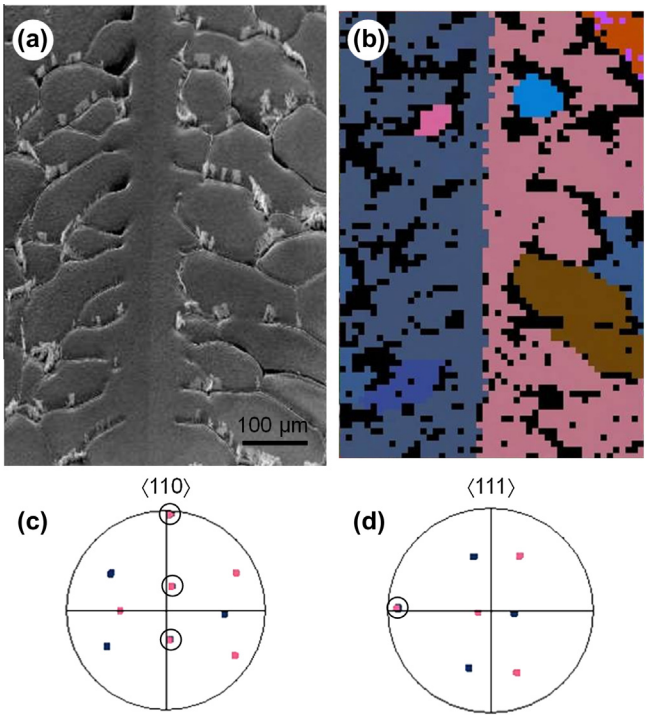

Fig. 4. (a) SEM image of a twinned dendrite in an ES Al–20 wt.% Zn–0.1 wt.% Cr alloy, with the {1 1 1} twin plane now perpendicular to the figure. (b) EBSD relative Euler orientation map of the region in (a). (c) ⟨1 1 0⟩ and (d) ⟨1 1 1⟩ pole figures of the twinned lamellae. In these pole figures, the common ⟨1 1 0⟩ and ⟨1 1 1⟩ directions are circled.

of 7–8° around a common ⟨1 1 0⟩ direction in this plane. It should be noticed that twinned and near-twinned pairs of grains are adjacent to each other and present reentrant corners at their triple lines with the surrounding quenched liquid.

Since pairs of equiaxed twinned grains were found in Al–20 wt.% Zn–0.1 wt.% Cr, a detailed investigation was carried out to determine the density of twins of adjacent grains in this alloy. For that purpose, an extensive EBSD analysis was performed for an area of 2 mm × 20 mm, using a 10 μm step size. A part of the EBSD map is shown in Fig. 6. The 2468 grains present in the reconstructed map exhibit 6422 grain boundaries. We then defined the "twin-relationship tolerance" of two neighboring grains as: (i) the maximum acceptable deviation of one of their nearly common ⟨1 1 1⟩ directions; (ii) the maximum acceptable deviation of one of their nearly common ⟨1 1 0⟩ directions. Setting this twin-relationship tolerance to 5°, we have found that 150 out of the 6422 boundaries are in twin relationship, i.e., a frequency of 2.3%. These boundaries are highlighted with white segments in Fig. 6. Taking a random orientation of a grain with respect to a reference grain, the probability to be in a twin relationship within the 5° tolerance can be calculated according to Ref. [24]: it is equal to 0.3%, i.e., an order-of-magnitude less than the value found experimentally.[2] This clearly proves that the occurrence frequency of twin boundaries in ES Al–20 wt.% Zn–0.1 wt.% Cr alloys is not due to random nucleation. And it concerns only nearest-neighbor grains, since we did not try to establish twin or nearly twin relations with second- or third-nearest neighbors. It should also be noted that there are several grains in the specimen having multiple twin relationships, which have even much lower probability of occurrence for a population of randomly nucleated grains. These specific cases are analyzed in detail later.

When the twin-relationship tolerance is set to 5°. for the identification of twin boundaries, the near-twinned grains shown in Fig. 5e and f (rotation of ~7–8° of the ⟨1 1 1⟩ direction along a common ⟨1 1 0⟩ direction) are not included in the statistics calculated before. However, in the present study, they are considered to be of particular significance for understanding the formation mechanism of twins in Al alloys. Indeed, a 7–8° rotation of {1 1 1} planes along a common ⟨1 1 0⟩ direction is the angular opening of the gap that forms when a ring of five regular tetrahedra sharing an edge is formed, as illustrated in Fig. 7a.

Regular tetrahedra in an fcc crystal have four {1 1 1} triangular facets and six ⟨1 1 0⟩ edges. Two adjacent tetrahedra (except the first and the last ones in this figure) have a perfect twin relationship with a common {1 1 1} twin plane, and all the five crystals rotate around a common ⟨1 1 0⟩ direction. However, because the angle between two {1 1 1} planes is 70.53°, just short of the 72° required for a perfect fit into a pentagonal dipyramid, there is a 7.35° gap between the closest {1 1 1} planes of the first and the last tetrahedra of Fig. 7. This situation closely corresponds to the near-twin relationship observed for the pairs of grains 3 and 4 in Fig. 5e and f, respectively: a ⟨1 1 0⟩ direction and two {1 1 1} planes rotated by 7–8°.

The fivefold symmetry of the pentagonal dipyramid being essentially the same in the icosahedron which is the basis of QCs mainly observed in Al alloys, it appears reasonable to question whether the twinned or near-twinned equiaxed grains observed in Al–20 wt.% Zn–0.1 wt.% Cr form on QCs or a crystalline phase exhibiting fivefold symmetry building blocks. More precisely, the α-phase would form from the facets of the icosahedron shown in Fig. 7, with the {1 1 1} planes and ⟨1 1 0⟩ directions corresponding to facets and edges of the tetrahedra, respectively. This hypothesis is further substantiated in the next section, after presenting briefly the literature related to QCs.

4. Discussion

4.1. Icosahedral quasicrystal (iQC) phase

While discussing the large undercoolings of pure metals measured by Turnbull [25], Frank [26] already proposed an icosahedral short range order (ISRO) of atoms in liquid metals. About 30 years after this hypothesis was put forward, the first QC, a solid atomic arrangement with rotational symmetry of the icosahedral point group and

[2] Defining a confidence interval of 99%, we find that the value of 2.3% has an error of ±0.5%.

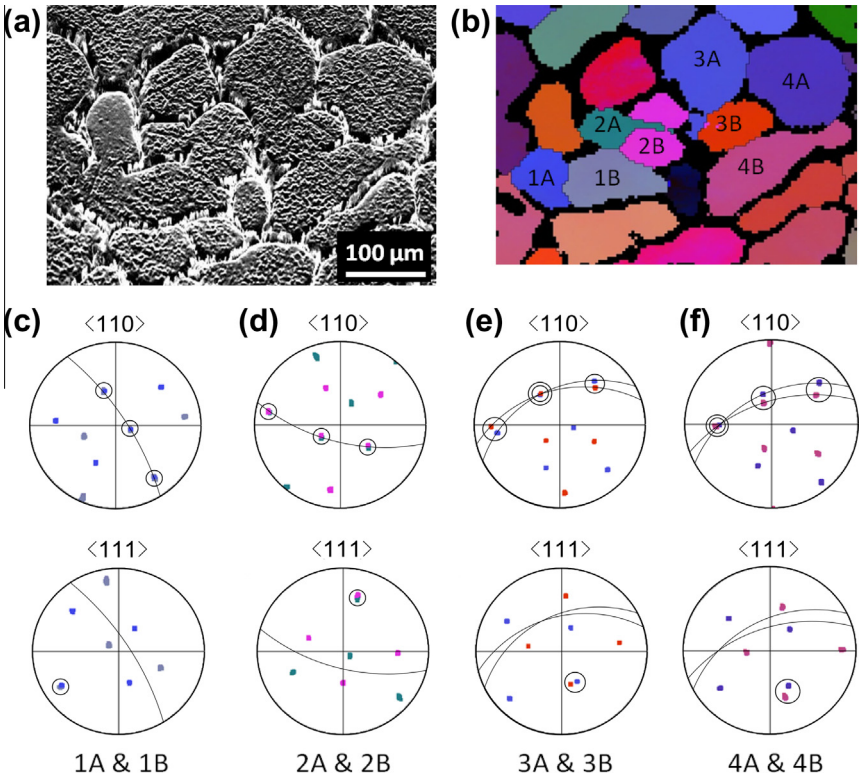

Fig. 5. (a) Microstructure of an Al–20 wt.% Zn–0.1 wt.% Cr alloy solidified under ES conditions. (b) EBSD relative Euler orientation map of the microstructure shown in (a). The corresponding ⟨1 1 0⟩ and ⟨1 1 1⟩ pole figures of pairs of grains numbered 1 to 4 are shown below: (c) 1A and 1B, (d) 2A and 2B, (e) 3A and 3B and (f) 4A and 4B. The common ⟨1 1 0⟩ and ⟨1 1 1⟩ directions corresponding to exact or slightly rotated {1 1 1} twin planes are highlighted with a circle, while the common ⟨1 1 0⟩ direction for near-twins are double circled.

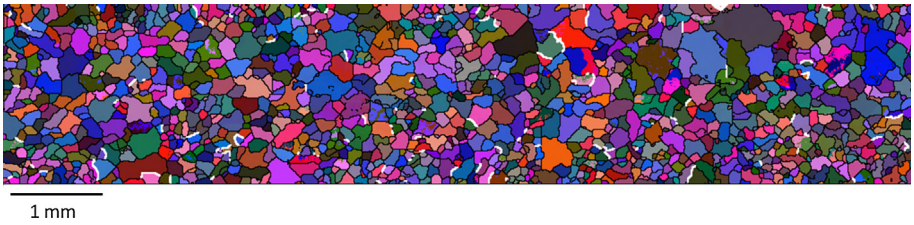

Fig. 6. EBSD relative Euler angle map of an ES Al–20 wt.% Zn–0.1 wt.% Cr alloy. White lines at grain boundaries indicate twinning relationship between the adjacent grains.

without long range translational order, was discovered by Shechtman et al. [27] in rapidly quenched Al–Mn alloy. While the concept of ISRO has been confirmed by molecular dynamics simulations [28,29], experimental indications of ISRO have recently been obtained by neutron diffraction [30,31] and by X-ray scattering [32] studies of undercooled metallic liquids. In experimental studies of Ti–Zr–Ni alloy, it was also demonstrated that ISRO acts as a template in the liquid and promotes the nucleation of metastable iQCs [33].

iQCs have been found mostly in Al–transition metal alloy systems [34]. They are generally metastable in binary Al alloys and form under rapid solidification conditions, but there are some ternary alloys such as Al–Pd–Mn [35], Al–Fe–Cu [36] and Al–Cu–Li [37] that are more stable than the competing crystalline phase and can be produced under

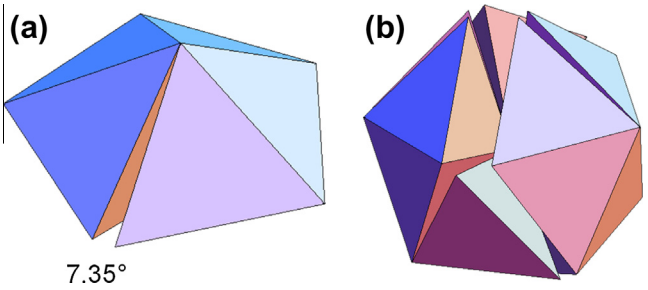

Fig. 7. (a) A ring of five tetrahedra sharing an edge forms almost a pentagonal dipyramid, but leaves a gap with an angle of 7.35°. (b) Construction of an icosahedron from 20 regular twinned tetrahedra.

equilibrium solidification conditions. While QCs generally nucleate homogeneously from the liquid, they also occur

as precipitates in different alloys, such as Al–Li–Cu and stainless steel [34]. Several metastable QCs have been observed in binary Al–X 3d transition alloys, where X = V, Cr, Mn, Fe, Co and Ni [21].

QCs generally exist together with crystalline and amorphous phases. They can in fact contribute significantly to their formation by acting as nucleation sites with some mutual crystallographic relationships [38]. In rapidly solidified and subsequently annealed Al–Cr alloys, Zhang et al. [39] reported that the [1 0 1] direction of the monoclinic $Al_{45}Cr_7$ phase is parallel to the fivefold axis of the icosahedral phase and found multiple twinning of $Al_{45}Cr_7$ around this axis. In as-quenched Al alloys, iQCs are frequently surrounded by the α-Al matrix. Crystals have various orientation relationships with QCs in order to form low energy interfaces by matching close packed planes. Guo et al. [40] have found three different orientation relationships and the existence of a coherent interface boundary between the icosahedral phase and the Al matrix in Al–Mn–Cr–Si alloy. Koskenmaki et al. [41] have observed twinned α-Al crystals forming an overall QC symmetry in a melt spun Al–Mn–Si alloy. Lüscher et al. [42] have also observed fivefold twinning of vapor deposited Al domains on the iQC Al–Pd–Mn surface.

4.2. More evidence of nucleation of twinned primary phase grains on a QC phase

The similarity between the orientation relationships of twinned or near-twinned grains found in Al–Zn–Cr (Fig. 5) and the packed five tetrahedra of a pentagonal dipyramid (Fig. 7a) motivated us to further investigate such specimens and find out if five mutually twinned crystals around a common ⟨1 1 0⟩ direction could exist.

Fig. 8a shows the EBSD reconstructed map of five grains, numbered 1 to 5, having twin or near-twin relationships with each other. Their mutual twin orientations are shown in five separate ⟨1 1 0⟩ pole figures (Fig. 8b–f), with in each case an arc of a circle corresponding to their nearly common {1 1 1} plane. The color code used to draw the pole figures is the same as that used in the reconstructed microstructure. As can be seen, twin or near-twin relationships exist between grains 1 and 2 (b), 2 and 3 (c), 3 and 4 (d), 4 and 5 (e), and finally 5 and 1 (f). The assemblage of the five experimental pole figures is shown in Fig. 8g and to help the reader, schematic orientation relationships between adjacent grains have been drawn in Fig. 8h with the same color code. All crystals are rotated around a common ⟨1 1 0⟩ direction (circles in g) and thus seem to have nucleated from a template possessing a fivefold rotational symmetry, such as that of an iQC.

As can be seen in Fig. 8, each grain exhibits fairly large misorientations (as measured by the spread of each EBSD orientation), in particular the red grain 2 which is the largest. This makes the fivefold symmetry not as perfect as could be expected. However, it should first be kept in mind that the assemblage of 20 tetrahedra into a single icosahedron overall exhibits larger misorientations as compared with the 7.35° of a pentagonal dipyramid (see Fig. 7b). Secondly, it is well known that misorientations due to solute segregation during solidification or strains induced during cooling can occur.

Another example of fivefold twinned or near-twinned crystallography relationship between several grains is provided in Fig. 9, where the mean orientation of each grain in this case has been plotted. The ⟨1 1 1⟩-pole figure shown in Fig. 9c clearly reveals the configuration of the five pairs of common {1 1 1} twin planes of the five grains, and of the

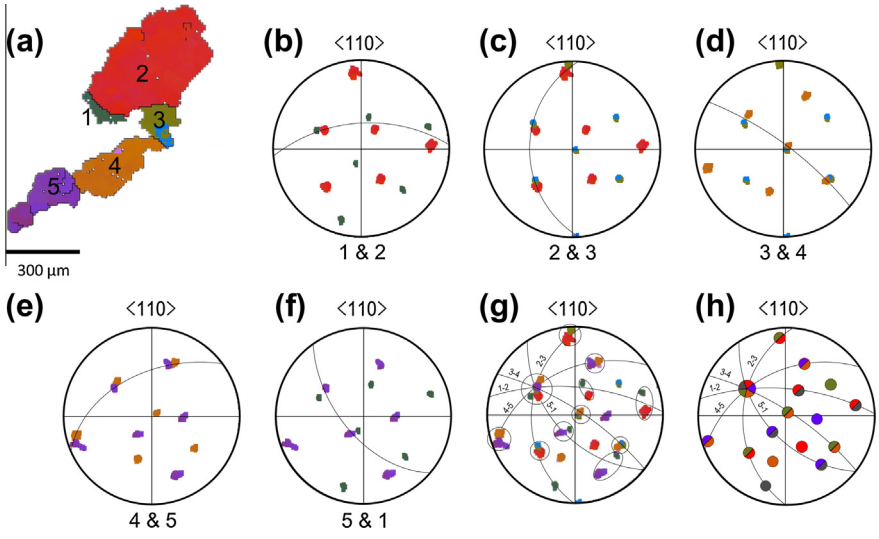

Fig. 8. (a) EBSD map of five grains in ES Al–20 wt.% Zn–0.1 wt.% Cr showing a fivefold twin symmetry relationship between pairs of grains, as demonstrated by the ⟨1 1 0⟩-pole figures shown in (b–f). A global ⟨1 1 0⟩-pole figure is shown in (g) whereas twin relationships can be seen more easily on the schematically drawn pole figure shown in (h) with the same color code. The common {1 1 1} planes are displayed in each pole figure by arcs of circle.

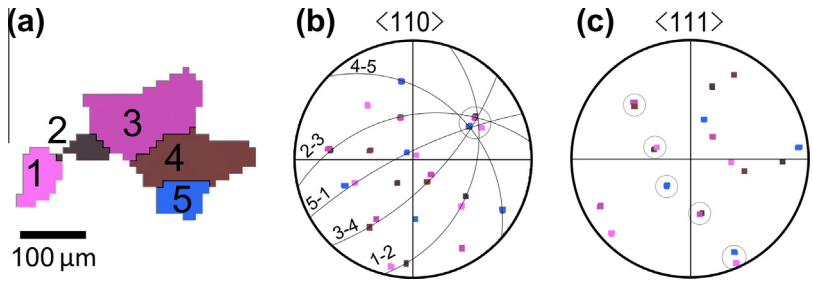

Fig. 9. (a) EBSD map of Al–Zn–Cr alloy showing fivefold twinned crystals and corresponding (b) ⟨1 1 0⟩- and (c) ⟨1 1 1⟩-pole figures. Common and close directions are circled on pole figures. The common {1 1 1} planes are shown by arcs of circle in (b).

10 other non-common {1 1 1} planes, with a fivefold rotation symmetry around the (essentially) common ⟨1 1 0⟩ direction (circled in Fig. 9b).

Even more interesting is the case shown in Fig. 10a, where four grains, labeled 1 to 4, have been enlarged from the large EBSD map shown in Fig. 6. Their ⟨1 1 0⟩, ⟨1 1 1⟩ and ⟨2 1 1⟩ pole figures are given in Fig. 10b, c and d, respectively. As can be seen from these pole figures, the grain pairs (1–2) and (3–4) are in a twin relationship, and their boundaries have been highlighted in light blue in Fig. 10a. The common ⟨1 1 0⟩- and ⟨1 1 1⟩-directions of these two pairs are circled in Fig. 10b and c, while an arc of circle identifies their common {1 1 1} plane. But twinning is not the only relationship existing between these four grains: indeed, the two pairs of grains (1–2) and (3–4) share a common ⟨2 1 1⟩ direction (circled in Fig. 10d) and their crystallographic configurations are simply rotated by 63° around this direction. Furthermore, grains 1 (violet) and 4 (blue) share one common ⟨1 1 0⟩ direction (circled in green in the pole figure, 10b), while grains 2 (green) and 3 (purple) share another ⟨1 1 0⟩ direction (circled in red in the same pole figure).

The very specific crystallographic relationships between these four grains can be understood if one considers the four triangular facets labeled 1–4 of the interlocked icosahedron shown in Fig. 10e. Assuming again to have epitaxial growth of the α-phase on the facets of this interlocked icosahedron, i.e., the {1 1 1} planes and ⟨1 1 0⟩ directions of the α-phase coincide with the facets and edges of the tetrahedra, one sees that: (i) tetrahedra 1 and 2, as well as 3 and 4, are in a twin relationship; (ii) tetrahedra 2 and 3 share a common ⟨1 1 0⟩ edge (in red); (iii) tetrahedra 1 and 4 have two parallel ⟨1 1 0⟩ edges (in green); (iv) all four tetrahedra have one parallel ⟨2 1 1⟩ direction, pointing outward of the interlocked icosahedron through the middle of one of their ⟨1 1 0⟩ edges (labeled with a small dot symbol). In summary, there is fairly clear evidence that an interlocked icosahedron must act as a template for the early nucleation stage of the four fcc α-grains in Fig. 10a.

4.3. Thermodynamic and final arguments

All the experimental results presented so far strongly suggest that a fivefold symmetry iQC and/or an equivalent phase with fivefold symmetry building blocks play a role in the nucleation of the primary α-phase in Al–20 wt.%Zn–0.1 wt.% Cr. The isothermal section at 635 °C of the Al–Zn–Cr ternary phase diagram predicted by ThermoCalc near the Al-rich corner further consolidates these results. As can be seen in Fig. 11a, the composition of our alloy (red dot) falls within the liquid-$Al_{45}Cr_7$[3] two-phase region at this temperature, before the fcc phase forms. This intermetallic phase has a monoclinic structure, with a very large unit cell containing 14 Cr and 90 Al atoms [43,44] (Fig. 11b). Several icosahedral building blocks formed by a Cr atom at the center of 12 Al atoms (Al or Zn) at the vertices can be seen. These icosahedral building blocks are linked together by sharing a vertex, an edge or a face, or by interlocking (see Fig. 10e). The mean interatomic distance between Al atoms, which mainly constitute the outer shell of the icosahedra, is 2.85 Å [43]. It should be noted that this value is very close to the interatomic distance between Al atoms in {1 1 1} planes of the fcc phase.

Although there has been no study on QC formation in Al–Zn–Cr alloys, Al–Cr is one of the first binary systems in which QCs were observed [27]. Al and Cr have the appropriate atomic radii to be arranged in the icosahedral configuration and besides $Al_{45}Cr_7$, other Al-rich intermetallic compounds formed by peritectic reactions, $Al_{11}Cr_2$ and Al_4Cr, have also icosahedral atomic arrangements in their unit cell [45]. These complex intermetallics formed under equilibrium conditions can coexist together with iQCs in rapidly solidified Al–Cr alloys when there is insufficient time for long range ordering [21,39,46]. Also in Al–Zn–Cr alloys, an intermetallics phase, $Zn_{13}(Cr_xAl_{1-x})_{27}$ ($x = 0.34$–0.37), has been recently reported which has icosahedral building blocks in its rhombohedral structure [47]. Therefore, the existence of the complex $Al_{45}Cr_7$ and $Zn_{13}(Cr_xAl_{1-x})_{27}$ ($x = 0.34$–0.37) intermetallic phases at equilibrium is also an indication of the tendency to form icosahedral ordering in Al–20%Zn–0.1%Cr alloy.

As already discussed, iQC is a metastable phase between the liquid and the stable crystalline phase, which can nucleate and grow if the cooling rate is small enough to allow its

[3] The composition of this Al-rich intermetallic phase is also described as $Al_{13}Cr_2$ and Al_7Cr.

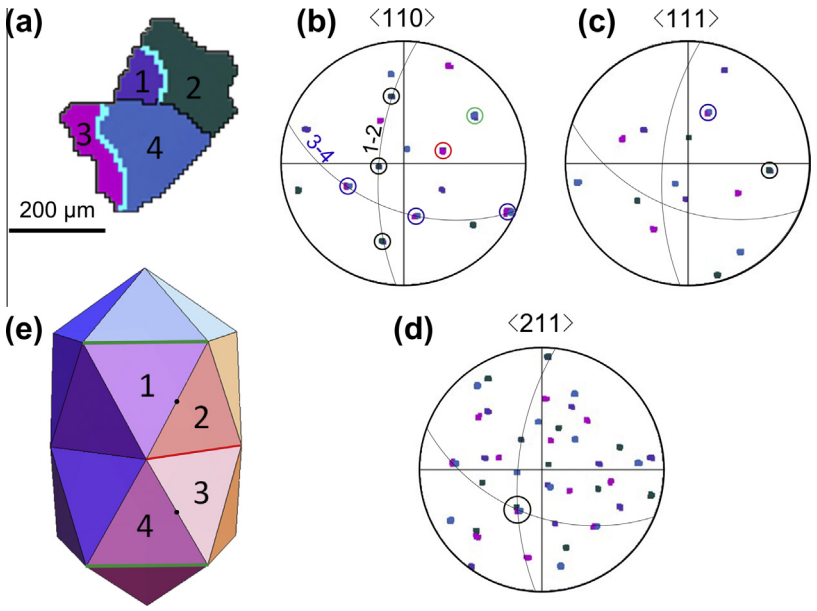

Fig. 10. (a) EBSD map reconstructed with the Euler angles of four isolated crystals of Fig. 6. Light blue boundaries highlight the presence of a twin relationship. The ⟨1 1 0⟩, ⟨1 1 1⟩ and ⟨2 1 1⟩ pole figures of these grains are shown in (b), (c) and (d), respectively. Common {1 1 1} planes between grains 1–2 and 3–4 are shown by an arc of a circle on the pole figures. The common ⟨2 1 1⟩ to all four grains is circled in (d). (e) Schematics of an interlocked icosahedron showing the four facets 1–4 on which {1 1 1} planes of the four Al grains seen in (a) can form to explain their orientation relationship. The common edge between 2 and 3 (in red) and common parallel edge between 1 and 4 (in green) correspond to the common ⟨1 1 0⟩ directions in the pole figure (b) circled with the same color.

formation and large enough to inhibit the formation of the equilibrium phase [27]. After nucleation of the icosahedral phase, crystalline phase starts to form by preserving the orientational order of the underlying icosahedral symmetry, as suggested by Bendersky et al. [48] and Srivastava and Ranganathan [49]. The mechanism by which the α-phase then forms on such iQC with multiple twins is schematically shown in Fig. 12 for a simple two-dimensional situation. It assumes that the initial formation of the iQC nucleus in the undercooled liquid is followed by the "nucleation", or growth, of α-Al crystals on the facets of the iQC with corresponding crystallographic relationships. In other words, the iQC acts as a template for the formation of many fcc grains having then twin or near-twin relationships between them.

The icosahedral phase cannot grow over long distances and generally exists as small clusters with a high surface-to-volume ratio. During growth, there are two possible sites to build the next layer: (i) icosahedral sites located above the edges of the icosahedron, i.e., along ⟨1 1 0⟩ directions of the tetrahedra making the icosahedron; (ii) closed-packed sites located above the center of each triangular face of the icosahedron. Icosahedral sites should be preferred to cover a large surface and to preserve the icosahedral symmetry, but are energetically unfavorable due to their position [50]. If close packed sites are occupied with atoms during the growth, a transition from icosahedral to fcc structures will occur [51]. The α-Al phase then grows with an orientation given by that of the icosahedron, i.e., the external facets and edges of the icosahedron correspond to {1 1 1} planes and ⟨1 1 0⟩ directions, respectively, with twin or near-twin relationships in between each fcc grain. There is an energy balance between the twin boundary energy, the solid–liquid interfacial energy and the elastic strain involved to compensate for the closure default of the icosahedron. This situation share then some similarities with multi-twinned nano-particles of Au and Ag studied in the 1960s [52,53]. When the multi-twinned grain reaches a certain radius, the solid–liquid interface destabilizes and can lead to the formation of twinned dendrites. Since the Al–Cr system is peritectic, the icosahedral phase may transform into the stable α-Al phase once the temperature falls below the peritectic temperature.

Another supportive point of the proposed mechanism, which implies the presence of an icosahedral phase during the nucleation stage of twinned α-Al crystals, is the parallelism between the formation conditions of QCs and twinned dendrites. Although some QCs might form under fairly low cooling rate, their formation probability increases with the cooling rate (typically above 100 K s^{-1}) [54]. This is also the case for the formation of twinned dendrites.

5. Conclusion

For the first time, the formation of twinned dendrites under equiaxed solidification conditions, without inoculation and with limited convection, has been observed in Al–20 wt.% Zn–0.1 wt.% Cr. This could definitely be attributed to the addition of a few chromium atoms. Besides the

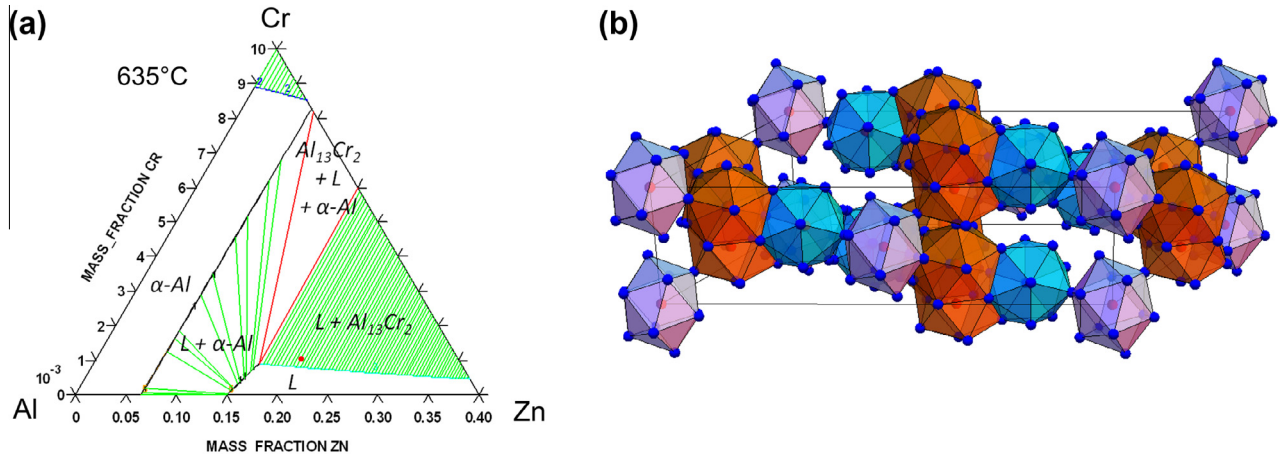

Fig. 11. (a) 635 °C isothermal section of the Al–Zn–Cr ternary phase diagram calculated with ThermoCalc, near the Al-rich corner. The composition of the alloy (20 wt.% Zn–0.1 wt.% Cr shown with a red dot indicates that the first phase to form is the $Al_{13}Cr_2$ intermetallics and not the α-Al phase. (b) Crystal structure of $Al_{45}Cr_7$ drawn with the atomic coordinates of Ref. [43]. While Al atoms are shown in blue, Cr atoms at the center of icosahedral clusters are shown in red. (For interpretation of the references to color in this figure legend, the reader is referred to the web version of this article.)

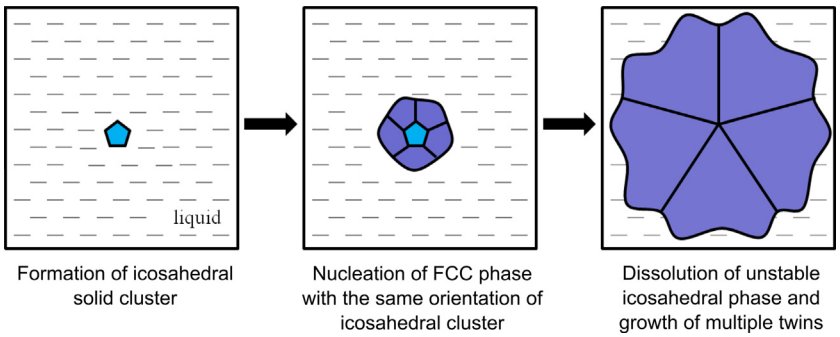

Fig. 12. Schematic diagram of the possible mechanism leading to the formation of α-Al multiple twinned grains from an existing icosahedral phase in the liquid. While light blue represents the icosahedral phase, deep blue shows the crystalline fcc phase. (For interpretation of the references to color in this figure legend, the reader is referred to the web version of this article.)

formation of a long twinned dendritic grain, it has been shown that minute Cr additions drastically refine the grain size of this alloy and furthermore induce an abnormal number of twin or near-twin relationships between nearest-neighbor grains. This is already fairly puzzling since Al is known to have a fairly high stacking fault energy compared to that of other metals. Besides twinning, pairs of grains sometimes show near-twin relationships with a rotation of the near-common {1 1 1} plane by ~7° around a common ⟨1 1 0⟩ axis. Several sets of grains are shown to have orientation relationships compatible with the icosahedron or interlocked icosahedron geometry.

All these findings are fairly strong evidences that a fivefold symmetry template similar to that of iQC promotes the formation of the fcc phase, even though no icosahedral or $Al_{45}Cr_7$ phase was observed in the present study. This novel "nucleation" mechanism (but is it nucleation? or should we rather talk about heteroepitaxial growth on a template?) is further supported by several considerations: (i) icosahedral short range order in undercooled metallic liquids is proven; (ii) icosahedral solid clusters in Al–Zn–Cr melts tend to form due to the presence of stable phases such as $Al_{45}Cr_7$ and $Zn_{13}(Cr_xAl_{1-x})_{27}$ ($x = 0.34$–0.37) in this system, which have icosahedral building blocks in their unit cells; (iii) there are many examples in the literature for the growth of multiple twins of intermetallics from an icosahedral phase and the same can well be possible for the multiple twin formation of stable α-Al crystals; (iv) the conditions under which iQCs form are quite similar to those favoring the appearance of twinned dendrites in industrial Al alloys (high cooling rate, presence of Fe impurities which are inherent to aluminum and can favor QC formation).

Nucleation of α-Al crystals on pre-existing icosahedral solid clusters in the liquid provides an explanation for the nucleation of twinned dendrites in Al alloys. But even more important, it indicates that the addition of minute elements favoring the formation of an icosahedral phase could bring a significant contribution to nucleation phenomena, and explain why current rationales do not predict the detail of grain refinement of the different aluminum alloys, even when constitutional undercooling has been carefully

accounted for. This has been shown to be the case of Al–20 wt.%Zn when 0.1 wt.% Cr is added, but it is highly probable that the same mechanism could operate for other metallic alloys.

Acknowledgements

The authors thank Constellium Research Center at Voreppe for its financial support. They also thank the staff of the Centre Interdépartemental de Microscopie Electronique (CIME) of the Ecole Polytechnique Fédérale de Lausanne (EPFL) and in particular Dr. E. Boehm-Courjault for their assistance with the EBSD measurements. Phase diagram calculations of L. Rougier and technical assistance of J.-D. Wagnière are gratefully acknowledged. The authors also wish to thank Professor J.A. Dantzig for fruitful discussions.

References

[1] Herenguel J. Rev Metall 1948;45:139.
[2] Mondolfo LF. Metallography of aluminum alloys. New York: Wiley; 1943.
[3] Henry S, Jarry P, Jouneau PH, Rappaz M. Metall Mater Trans A 1997;28:207.
[4] Henry S, Jarry P, Rappaz M. Metall Mater Trans A 1998;29:2807.
[5] Henry S, Minghetti T, Rappaz M. Acta Mater 1998;46:6431.
[6] Henry S, Gruen GU, Rappaz M. Metall Mater Trans A 2004;35:2495.
[7] Salgado-Ordorica MA, Rappaz M. Acta Mater 2008;56:5708.
[8] Turchin AN, Zuijderwijk M, Pool J, Eskin DG, Katgerman L. Acta Mater 2007;55:3795.
[9] Morris LR, Carriuthers JR, Plumtree A, Winegard WC. Trans TMS-AIME 1966;236:1286.
[10] Gonzales F, Rappaz M. Metall Mater Trans A 2006;37:2797.
[11] Haxhimali T, Karma A, Gonzales F, Rappaz M. Nat Mater 2006;5:660.
[12] Salgado-Ordorica MA. PhD thesis, #4568, Ecole Polytechnique Fédérale de Lausanne, Lausanne, Switzerland; 2009.
[13] Li L, Zhang Y, Esling C, Zhao Z, Zuo Y, Zhang H, et al. J Cryst Growth 2009;311:3211.
[14] Eady JA, Hogan LM. J Cryst Growth 1974;23:129.
[15] Wood HJ, Hunt JD, Evans PV. Acta Mater 1997;45:569.
[16] Napolitano RE, Liu S. Phys Rev B 2004;70:214103.
[17] Salgado-Ordorica MA, Burdet P, Cantoni M, Rappaz M. Acta Mater 2011;59:5085.
[18] Salgado-Ordorica MA, Desbiolles JL, Rappaz M. Acta Mater 2011;59:5074.
[19] Friedli J, Di Napoli P, Rappaz M, Dantzig JA. Mater Sci Eng 2012;33:012111.
[20] Kurtuldu G, Rappaz M. Ecole Polytechnique Fédérale de Lausanne, Lausanne, Switzerland, unpublished research; 2011.
[21] Grushko B, Velikanova TYa. Powder Metall Met Ceram 2004;43:72.
[22] Salgado-Ordorica MA, Phillion AB, Rappaz M. Metall Mater Trans A 2013;44:2699.
[23] Vandyoussefi M, Greer AL. Acta Mater 2002;50:1693.
[24] Warrington DH, Boon M. Acta Metal 1975;23:599.
[25] Turnbull D. J Appl Phys 1950;21:1022.
[26] Frank FC. Proc Royal Soc London A 1952;215:43.
[27] Shechtman D, Blech I, Gratias D, Cahn JW. Phys Rev Lett 1984;53:1951.
[28] Steinhardt PJ, Nelson DR, Ronchetti M. Phys Rev B 1983;28:784.
[29] Fang XW, Wang CZ, Yao YX, Ding ZJ, Ho KM. Phys Rev B 2011;83:224203.
[30] Simonet V, Hippert F, Audier M, Bellissent R. Phys Rev B 2001;65:024203.
[31] Holland-Moritz D, Schenk T, Bellissent R, Simnoet V, Funakoshi K, Merino JM, et al. J Non-Cryst Solids 2002;312–314:47.
[32] Reichert H, Klein O, Dosch H, Denk M, Honkimaki V, Lippmann T, et al. Lett Nat 2000;408:839.
[33] Kelton KF, Lee GW, Gangopadhyay AK, Hyers RW, Rathz T, Rogers J, et al. Phys Rev Lett 2003;90:195504.
[34] Kelton KF. Int Mater Rev 1993;38:105.
[35] Tsai AP, Inoue A, Yokoyama Y, Masumoto T. Mater Trans JIM 1990;31:98.
[36] Tsai AP, Inoue A, Masumoto T. J Mater Sci Lett 1987;6:1403.
[37] Dubost B, Lang J-M, Tanaka M, Sainfort P, Audier M. Nature 1986;324:48.
[38] Singh A, Tsai AP. J Phys Condens Matter 2008;20:314002.
[39] Zhang H, Wang DH, Kuo KH. Phys Rev B 1988;37:6220.
[40] Guo YX, Hoier R, Andersen S, Lohne O. Mater Sci Eng 1991;A134:1215.
[41] Koskenmaki DC, Chen HS, Rao KV. Phys Rev B 1986;33:5328.
[42] Lüscher R, Erbudak M, Weisskopf Y. Surf Sci 2004;569:163.
[43] Cooper MJ. Acta Cryst 1960;13:257.
[44] He ZB, Zou BS, Kuo KH. J Alloys Compd 2006;417:L4.
[45] Audier M, Durand-Charre M, Laclau E, Klein H. J Alloys Compd 1995;220:225.
[46] Bendersky L, Schaefer RJ, Biancaniello FS, Shechtman D. J Mater Sci 1986;21:1889.
[47] Thimmaiah S, Han M-K, Miller GJ. Z Kristallogr 2011;226:557.
[48] Bendersky LA, Cahn JW, Gratias D. Phil Mag 1989;60B:837.
[49] Srivastava AK, Ranganathan S. Acta Mater 1996;44:2935.
[50] Martin TP. Phys Rep 1996;273:199.
[51] Farges J, de Feraudy MF, Raoult B, Torchet G. J Chem Phys 1986;84:3491.
[52] Ino S. J Phys Soc Jpn 1966;21:346.
[53] Ino S. J Phys Soc Jpn 1969;27:941.
[54] Holland-Moritz D, Schroers J, Grushko B, Herlach DM, Urban K. Mater Sci Eng 1997;A226:976.